

# Development of a High-Current Low-Inductance Crowbar Switch for FRX-L

Chris Grabowski, James H. Degnan, *Senior Member, IEEE*, T. Cavazos, Donald G. Gale, C. Gilman, W. Sommars, Tom P. Intrator, J. Martin Taccetti, B. Waganaar, R. E. Siemon, and Glen A. Wurden, *Senior Member, IEEE*

**Abstract**—The design and test results of a crowbar switch developed for the formation of long-lifetime field-reversed configurations are presented. These research efforts are being pursued at the FRX-L facility at Los Alamos National Laboratory using the “Colt” capacitor bank (a 36  $\mu\text{F}$  Shiva Star bank module capable of storing up to 250 kJ) and at the Air Force Research Laboratory using the “Formation” capacitor bank (consisting of three parallel banks identical to Colt). The crowbar switch design includes four Maxwell rail-gap switches mounted on a cable header that transitions from the capacitor bank bus plates to 48 RG 17/14 coaxial cables. For the testing performed at AFRL, a dummy load was set up to simulate the magnetic field coils of the actual experiment. Tests thus far have demonstrated the crowbaring of peak currents up to 1.25 MA. Breakdown within the cable header due to the initial high voltage applied from the bank has been successfully suppressed by the cable feed-through design, proper placement of Mylar sheets around the switch for insulation, and replacement of air in the header with  $\text{SF}_6$ . Timing for the triggering of the crowbar is somewhat critical, as inductance in the switch increases when the switch is triggered with lower voltages across the switch rails. At the higher bank charge voltages, the charge-flow ratings on the rail-gap switches are exceeded; however, other than requiring that the rail electrodes in the switches be cleaned more frequently, no detrimental effects have been observed from the excessive charge flow.

**Index Terms**—Cable feedthroughs, crowbar switches, pulsed power, rail-gap switches, field-reversed configurations.

## I. INTRODUCTION

THE FIELD reversed configuration (FRC) is an elongated compact toroid of plasma that is formed without a toroidal magnetic field. As illustrated in Fig. 1, the structure of this configuration consists of a closed-field-line torus inside a separatrix and an open-field-line sheath outside the separatrix. A plasma that is formed and then compressed into this configuration offers many advantages for use as a “target” in magnetized target fusion (MTF) experiments. For example, the plasma may be created inductively, thus no internal electrodes are required that may introduce impurities, the field configuration results in a rather high plasma beta ( $\beta \sim 1.0$ ), and the separatrix acts as a natural diverter, isolating the plasma from the chamber walls

Manuscript received September 25, 2001; revised July 11, 2002. This work was supported by DOE-OFES.

C. Grabowski, T. Cavazos, D. Gale, C. Gilman, and W. Sommars are with the Science Applications International Corporation, Albuquerque, NM 87106 USA.

J. H. Degnan is with the Air Force Research Laboratory, Directed Energy Directorate, Kirtland AFB, NM 87117 USA.

T. P. Intrator, J. M. Taccetti, B. Waganaar, R. E. Siemon, and G. A. Wurden are with the Los Alamos National Laboratory, Los Alamos, NM 87545 USA.

Digital Object Identifier 10.1109/TPS.2002.805405

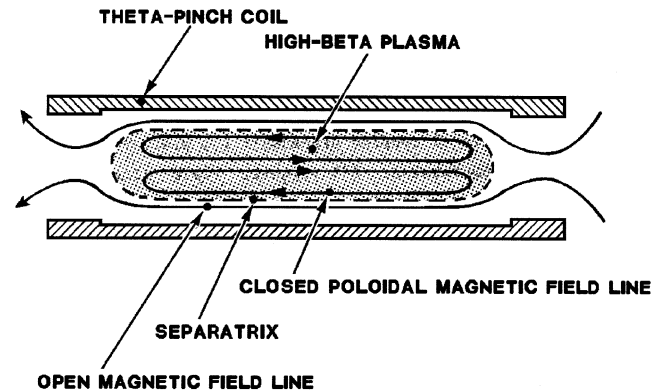


Fig. 1. Diagram of the FRC [1].

that can also be a source of impurities. In addition, earlier studies with FRCs (e.g., those described in [1]) have demonstrated that FRCs can be kept confined for a significant length of time and readily undergo axial translation after they are formed.

The formation of an FRC suitable for subsequent compression to MTF conditions [2] requires at least three capacitor bank discharges. For the planned experiments at Los Alamos National Laboratory (LANL) and at the Air Force Research Laboratory (AFRL) on Kirtland Air Force Base these bank discharges include: 1) a slow risetime discharge ( $\sim 100 \mu\text{s}$  to a few ms) to establish an approximately 0.3 to 0.5 T axial magnetic field in an approximately 10 cm diameter, 30-cm long theta discharge tube with a 50 to 100 mtorr deuterium prefill; 2) a much faster, modest energy, oscillating preionization discharge, with an amplitude comparable to the bias field; and 3) a more energetic reverse-field discharge with a risetime of 2 to 3  $\mu\text{s}$ , a much longer decay time, and an amplitude of approximately a factor of 10 greater than the initial bias field. One or more Shiva Star modules are being used to drive this third discharge, and this discharge must be crowbarred to allow for adequate time (10 to 20  $\mu\text{s}$ ) for subsequent compression and translation of the FRC. In addition to these three capacitor bank discharges, one or two additional bank discharges may be employed to maintain axial confinement or to facilitate the axial translation. A drawing in Fig. 2 shows the vacuum test chamber at the FRX-L facility at LANL and the arrangement around the test chamber of the different field coils driven by these capacitor bank discharges.

This paper focuses on the crowbar switch developed for crowbaring the reverse-field discharge in the experiments. The switch has already been designed, built, assembled, and tested at AFRL and has recently been moved to the FRX-L test facility at LANL and integrated into the FRC experiment there.

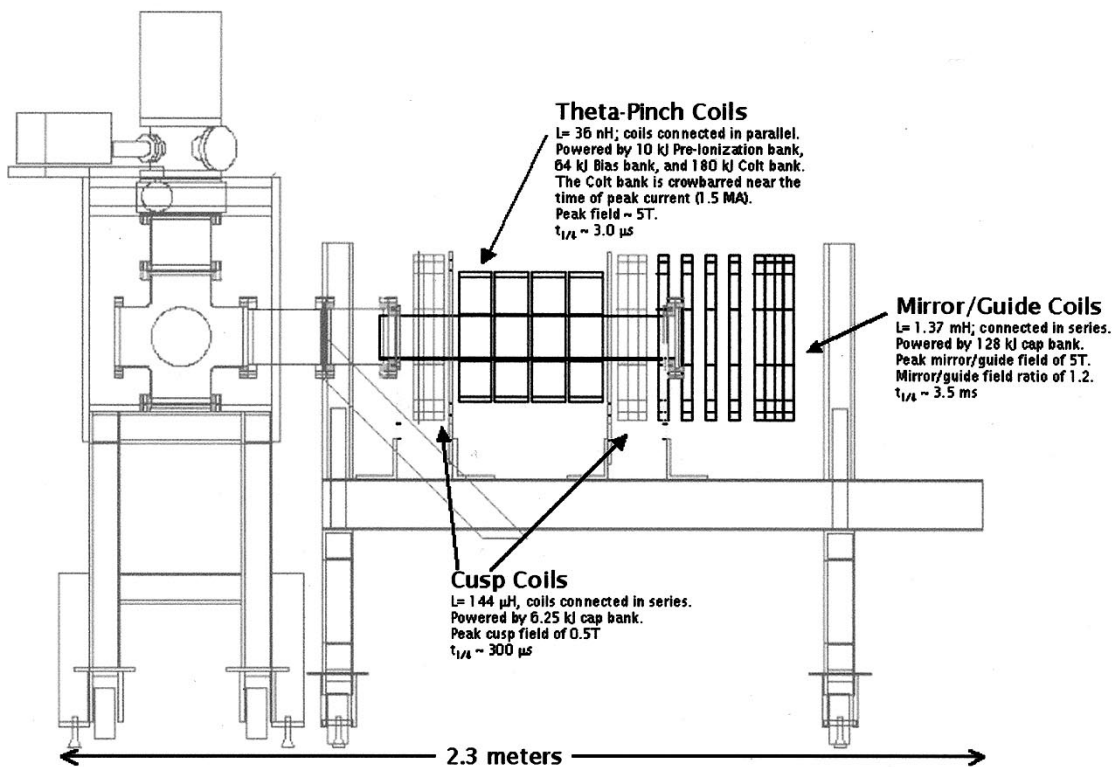


Fig. 2. Drawing of the vacuum test vessel at the FRX-L facility, showing the various sets of magnetic field coils that will be used to form, confine, and translate the FRC.

In this experiment, the transmission line connecting the Shiva Star module to the theta discharge coils includes a cable header section mounted to the module that converts from parallel plate to an array of forty-eight low-inductance coaxial cables. (Another cable header converts from coaxial cable back to parallel plate at the theta coils.) The crowbar switch shorts out the cable connections at the module as the discharge current approaches its peak value. During testing at AFRL, the crowbar switch was operated successfully for 80 kV, 1.25 MA discharges into a 40-nH test load. For the present, conservatively designed crowbar switch and connections, the oscillations superimposed on the crowbarred current are approximately  $\pm 25\%$ .

Section II of this paper presents the details and considerations that went into the design of the crowbar switch, as well as some special considerations required for the design of the cable header on which it is mounted. The crowbar switch tests at AFRL are then described in detail in Section III, and Section IV discusses some possible improvements in the design to lower switch inductance further. Finally, in Section V the overall operation of the switch is summarized, and some concluding remarks are made.

## II. CROWBAR SWITCH AND CABLE HEADER DESIGN

Several factors were prominent in influencing the design of the crowbar switch and the cable header on which it is mounted. The first is that it was desired to minimize the changes to be made to the existing Shiva Star module hardware. Clearly, having a low inductance in the overall crowbar switch circuit was desired, as well. However, one issue of particular concern

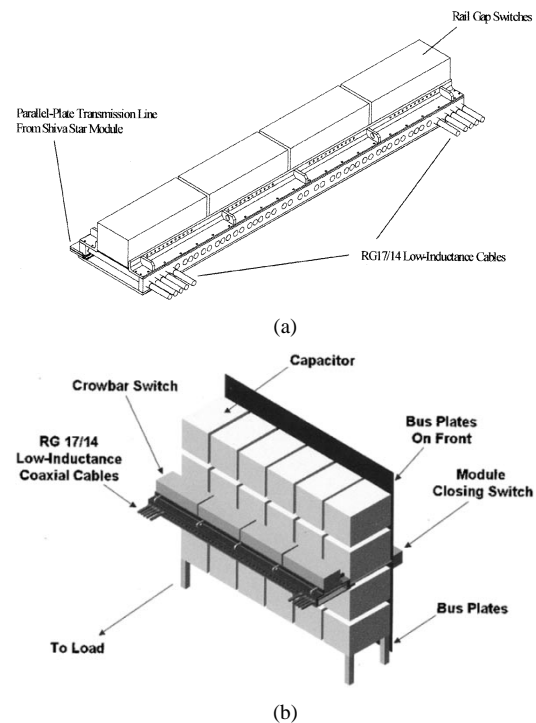


Fig. 3. (a) Illustration of the crowbar switch, its mounting hardware, and the cable header below the switch. (b) The crowbar switch and cable header shown mounted on the back of a Shiva Star module.

was surface flashover in the cable header. During previous experiments with the Shiva module at LANL (the "Colt" bank), flashover in the cable header on the bank was observed quite

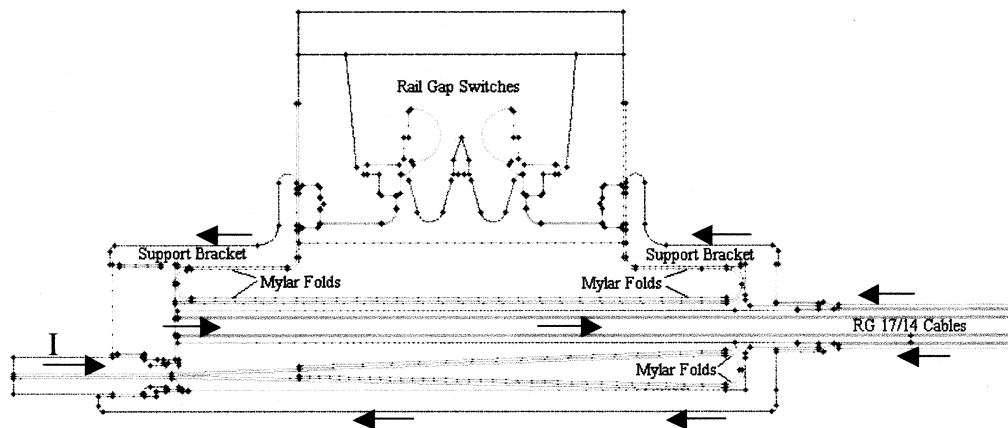


Fig. 4. Cross-sectional diagram of the crowbar switch and cable header. The arrows indicate how the current flows from the parallel plates into the header and then into the cables. When the crowbar switch is fired, the return current path from the load shifts from the bottom plate of the header to the brackets and rail-gap switches bridging the top of the header.

regularly when the bank was charged to voltages above 60~70 kV (composite charge voltage). In an effort to adequately address all of these design considerations, the design shown in Fig. 3(a) was developed. Fig. 3(b) illustrates how the crowbar switch and cable header are mounted to the back of the Shiva Star modules.

#### A. Hardware Design Overview

As indicated in both drawings of Fig. 3(a) and (b), the crowbar switch consists of a quad set of pressurized rail-gap switches. These switches are Maxwell Model 40 302 (“Atlas style”) switches, and this arrangement is actually very similar to that normally used for the closing switches on the Shiva Star modules. A cross-sectional diagram of the crowbar switch and cable header in Fig. 4 shows further details of the assembly. As can be seen here, the four rail gap switches are supported by two angle brackets that simply bolt onto the bus bars of the cable header. The purpose of the cable header, of course, is to direct the energy flow from the parallel plate transmission line of the module into 48 parallel RG 17/14 low-inductance coaxial cables. Arrows shown in the diagram in Fig. 4 indicate the direction of current flow into the header. Before the crowbar rail gaps are triggered, current returning from the load flows from the cable outer conductors down to the bottom plate of the cable header; after the crowbar is triggered, current flows from the cable braids up through the crowbar switch and then back to the cable center conductors. Spacing between the cables and the bottom plate and between the cables and the crowbar switch was kept at a minimum in an effort to keep the inductance of the header and the crowbar switch low. The other ends of the cables are then attached to another cable header at the load (the theta coils of the experiment). Although this design required that the existing cable header on the LANL Colt bank be replaced, no other modifications to the bank hardware were required.

In order to allow the rail-gap switches to be brought close to the cables in the header (and thereby reduce inductance), the rigid Lexan flashguard usually placed on the back of the switches has been removed and replaced with a flexible flashguard. This flexible flashguard is made up of 24 sheets of 5-mil Mylar, ~18 in long and with a width extending 12 in past the rail

gaps on each side. Twelve sheets of Mylar are sandwiched between the angle brackets and the rail gap housings on each side of the rail gap switches, and windows cut in the Mylar allow the current contacts on the angle brackets to make electrical contact with the switches. A bead of silicone RTV between the bottom edge of the rail gap housings and the innermost Mylar sheets on each side ensures that no tracking across the bottom of the rail gap housing can occur. The excess lengths of the Mylar sheets are then folded up under the switches in the cable header. (Mylar sheets from the parallel plate transmission line also extend out into the cable header, but these were cut to match the length of the header, unlike in the previous Colt cable header where the excess length was also folded back under the cables. This latter arrangement is actually what is illustrated in Fig. 4.)

To verify this design, the ability of the flexible flashguard to hold off a high potential placed across the rail-gap switch was tested in a scaled down assembly containing a single rail-gap element. After the rail gap was pressurized (with an SF<sub>6</sub>/Ar mixture) well above typical operating values to prevent it from firing, a high voltage power supply was connected to the two parallel plates on the test header, and a dc potential was applied across them. The potential was increased slowly up to 95 kV, and no flashover was observed on any of the Mylar surfaces or on the rail gap housing.

#### B. Field Analysis Around the Cable Feed-Throughs in the Cable Header

It should be noted that there were no cables attached to the bus bars of the cable header in the test just described. This fact is significant because arcing across the first cable header on the Colt bank (which of course had no crowbar mounted on top of it but which in size and separation of the bus bars is very similar to this test header) was observed quite regularly at voltages above 60~70 kV. Placing a loose plastic bag around the original Colt header and flowing SF<sub>6</sub> into the bottom of the header reduced the occurrences of arcing but was not found to suppress the arcing completely. The arcing has been of considerable concern because it is an issue that must be addressed not only for the crowbar cable header but also for several other similarly configured cable headers that have been or are being constructed for

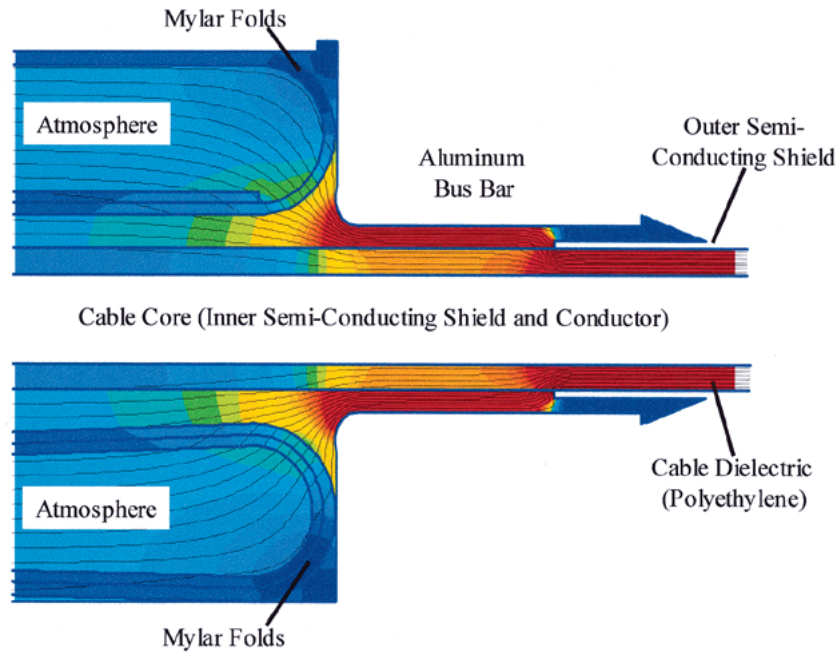


Fig. 5. Field map produced by QuickField showing an RG 17/14 coaxial cable within and emerging from the grounded cable bus bar on the crowbar cable header. Contour lines indicate constant potential, and the colored regions indicate electric field strength. The red regions show where fields are greater than 100 kV/cm; as the color transitions from red down to blue, the field intensity steadily decreases to zero. A potential of 80 kV is assumed here on the RG 17/14 center conductor.

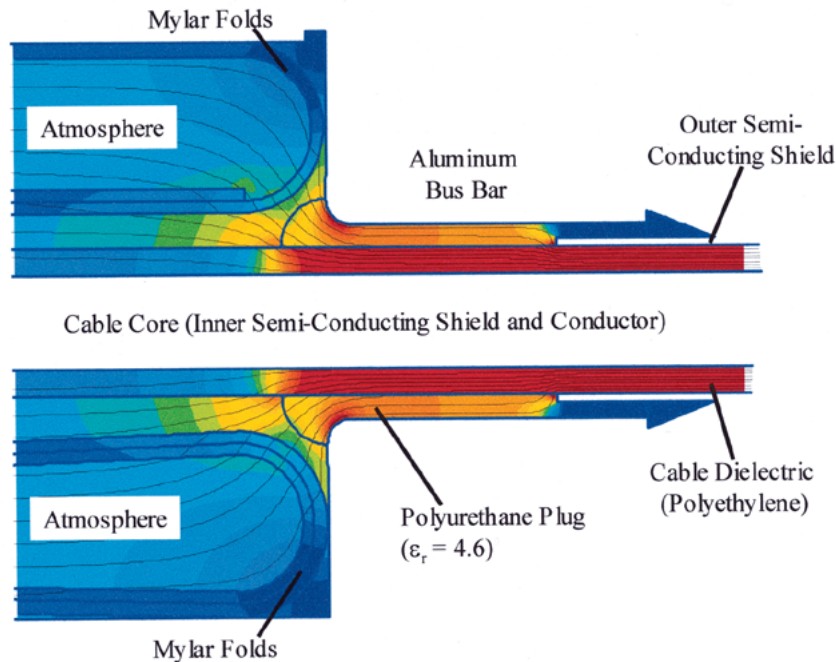


Fig. 6. This field map illustrates the changes in the field distribution around the cable that are produced by the insertion of a polyurethane plug. The color scale is the same as in the previous field map in Fig. 5.

the FRX-L experiment at LANL. Much emphasis was therefore placed, at both AFRL and at LANL, on determining the location(s) where the arcs originate and the path that they follow in an effort to suppress them.

The possibility of the arcs originating with trapped pockets of air breaking down between the Mylar layers (even after flooding the cable header with  $\text{SF}_6$ ) and then tracking along the Mylar surfaces was suggested first, since the folded Mylar layers in

the first header did come very close to the cables. However, in a conversation with personnel from Maxwell/Physics International (now Titan Pulse Sciences Division) the location where the cable dielectric and center conductor emerge from the bus bar was pointed out as being the most likely area for initiating the arc [3]. The radial field stresses at such locations, while maybe not being high enough to punch through the cable dielectric, are the highest here and can cause breakdown in the

surrounding atmosphere at or near the surface of the cable. Because the electric fields in the area where the cable emerges from the bus bar also begin to develop axial components a short distance from the bus bar, the plasma that is produced then readily spreads out along the surface of the cable dielectric, running toward the opposite cable bus bar and thereby propagating the arc.

In an effort to visually observe the process of arc development and determine whether the arcing was occurring between the Mylar sheets or along one of the cable dielectric surfaces, a small, four-cable mock-up of a cable header was assembled by several of the LANL FRX-L project personnel. A CCD camera with a fast shutter was used to provide a visual recording. In the mock-up, the Mylar sheets emerging from the parallel plates were cut to the width of the cable header and were therefore not folded back under the cables, as was done in the original Colt header, in an effort to keep them separated further from the cables. When the high potential bus bar of the header was pulsed with an impulse generator, arcing still occurred. The arc was observed to develop first across the thin gap between the cable dielectric and the grounded bus bar (the inner diameter of the bus bar hole was predefined by other mechanical considerations and was therefore slightly larger than the cable dielectric) and then to propagate toward the other bus bar, thus corroborating the descriptions suggested by the Maxwell/PI personnel.

Concurrent with the assembly of the cable header mock-up at LANL, numerical analyzes were being performed of the electric field intensities (electrostatic) in the crowbar cable header at AFRL. The cross-sectional diagram of the cable header and crowbar switch shown in Fig. 4 was used with QuickField, a finite element analysis program, to generate the field map that is shown in Fig. 5. A potential of 80 kV was placed on the cable center conductor in this particular analysis. The field map provides an enlarged view of the region where the RG 17/14 cable dielectric passes through and exits from the grounded bus bar in Fig. 4, and as is indicated in the map, the highest field strengths are observed to be in this region. The red shading designates areas where the electric field is 100 kV/cm and greater, and as the map color transitions from red to blue, the field steadily drops from 100 kV/cm down to zero. As was mentioned in the preceding paragraph, a thin air gap is present between the cable dielectric and the bus bar wall. This air gap concentrates much of the field in it after the outer semiconducting layer on the cable is terminated, and its presence actually reduces somewhat the field stresses directly on the surface of the cable as it exits from the bus bar. The highest fields are then actually found back inside the feedthrough at the triple point between the cable dielectric, the cable semiconductor layer, and the air.

The approximate breakdown field for this geometry and for air at Los Alamos (where the atmospheric pressure  $p \approx 565$  torr) is 32 kV/cm. This field strength is represented by one of the lighter shades of blue, and thus it is apparent that conditions favorable for air breakdown exist for quite some distance along the length of the cable after it exits the bus bar. As was noted previously, the Mylar layers from the parallel plates of the Shiva Star module (as they were arranged in the first Colt cable header), as well as those serving as the flashguard for the crowbar rail gaps, have been included in the diagram of Fig. 4 and were therefore also included in the electrostatic analysis.



(a)



(b)

Fig. 7. (a) Top and (b) side-on views of the crowbar rail gaps in place on top of the cable header. The photo in (b) shows how the Mylar sheets on either side of the rail gaps are folded up underneath and rest on top of the RG 17/14 cables. A gap of approximately 1 in. is left between the right set of Mylar sheets and the ground bus bar of the header to ensure that the air in this region is evacuated when the header is filled with SF<sub>6</sub>.

From Fig. 5 it appears that the fields are in fact high enough for breakdown to occur between the layers in the regions closest to the cable feed-through. However, as can be seen in the field map, the field intensities are considerably higher at the region where the cable exits the bus bar, and thus breakdown would likely occur there first.

By replacing the air with 100% SF<sub>6</sub>, a considerable advantage can be obtained in terms of the breakdown threshold: for a pressure of 565 torr and within this geometry, the breakdown field becomes approximately 87 kV/cm in SF<sub>6</sub>. However, the dark orange regions represent this field intensity, and there is still a region of red representing even higher fields that is found to extend out a

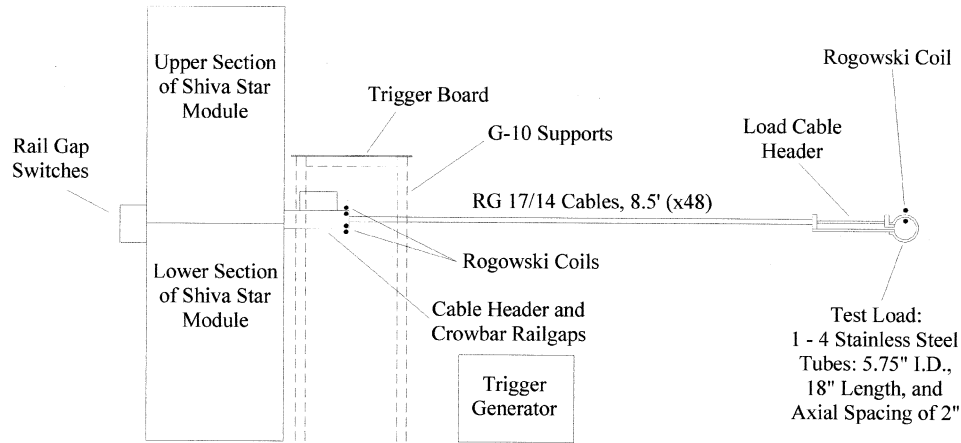


Fig. 8. Diagram of the test setup for the crowbar switch.

little from the bus bar along the cable. One possible way to raise the field at which breakdown occurs is to increase the pressure of the  $\text{SF}_6$  within the cable header. However, it becomes somewhat problematic not only to seal but also to reinforce such a large structure to handle any significant overpressure. Another solution is to somehow lower or redistribute the fields in and around the feedthrough, and this can be accomplished by inserting a material with a different dielectric constant into the gap around the cable. Fig. 6 shows a second field map of the crowbar cable header with a plug formed out of polyurethane now inserted around the cable dielectric. Because of the dielectric constant of the polyurethane ( $\epsilon_r = 4.6$ ), the electric field now transitions out of the cable dielectric very gradually. Furthermore, there are now no red regions in atmosphere, which implies that breakdown should now be completely suppressed provided that the air in the cable header is replaced with  $\text{SF}_6$ .

Based upon the results of the tests with the cable header mock-up and the findings from the numerical analyzes, the crowbar cable header design was tailored to include the placement of the polyurethane plugs around the cables. Dielectric grease placed on the inside surface of the plugs has been used to help eliminate any air gaps between the cable dielectric and the plugs. Furthermore, in order to allow a pure  $\text{SF}_6$  environment to be established within the cable header region, Lexan boxes were attached to both ends of the crowbar assembly to provide a seal at each end. As a means of determining the amount of  $\text{SF}_6$  within the header, a small hole was drilled into the top of one of the boxes, an 8-in-high tube was placed around the hole, and an air-filled balloon was then placed inside the tube. As the  $\text{SF}_6$  flowing into the header region begins to fill this region up, it starts to overflow into the tube on top of the box and causes the balloon to rise.

Fig. 7 shows two photos of the crowbar switch and cable header during assembly. The side-on view in Fig. 7(b) highlights the arrangement of the Mylar layers under the rail-gap switches and shows partially how the Lexan boxes are mounted onto the header.

### III. RESULTS FROM CROWBAR SWITCH TESTS

Testing and evaluation of the performance of the crowbar switch has been completed at AFRL, and in general the perfor-

mance was very good, meeting or even exceeding design expectations. Tests were successfully performed with the Shiva Star module charged to  $\pm 40$  kV (80 kV composite voltage), and, with adequate  $\text{SF}_6$  flow into the crowbar and test load cable headers, no evidence of breakdown was observed in either. Up to 1.25 MA of current was crowbarred in these shots, with the total charge flow through the crowbar switch in some shots exceeding 70 Coulombs.

However, oscillations in the crowbarred load current waveform were larger than anticipated. These oscillations are due to the inductance of the crowbar rail gaps and the other buss work of the switch, despite efforts to keep the inductance low. The effects of the crowbar switch inductance on the load current waveform can be reduced with higher load inductances and, of course, by making some modifications to the crowbar switch to further reduce its inductance. The test results, as well as some possible modifications that can be made to the switch to lower its inductance, are discussed in more detail below.

#### A. Crowbar Switch Currents

A diagram illustrating the crowbar switch test setup is shown in Fig. 8. An arrangement of 1 or 4 single-turn, stainless steel inductors, providing an inductance of approximately 40 nH or 10 nH, respectively, was used for the test load. (The actual inductance of the theta coils in the FRX-L experiment is  $\sim 36$  nH.) The cable header used with this test load is identical to the one under the crowbar switch. Diagnostics utilized during the tests were primarily Rogowski coils. Two Rogowski coils were located at the crowbar switch cable header: the lower one was used to measure the current flow from the Shiva module, and the upper one measured the current flowing through the crowbar switch. Two other Rogowski coils were placed at the same location around the test load but were oriented in opposite directions. By subtracting one signal from the other, any noise present in the signals could then be filtered out.

During this series of tests, the operation of the crowbar switch was evaluated for several different charge voltages on the Shiva Star module (from 30 kV to 80 kV composite voltage), for several different trigger delays (with respect to the triggering of the main discharge gaps on the module), and for the two different load inductances (10 nH and 40 nH). Fig. 9 shows the cur-

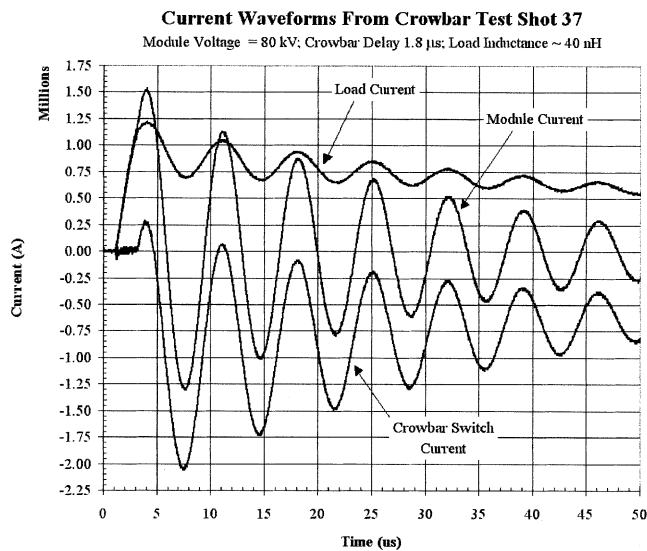


Fig. 9. Current waveforms obtained from the Rogowski coil signals from Test Shot 37. Analysis of the load current waveform shows that the ratio of the first current minimum to the initial current peak  $R_i$  is 0.579.

rent waveforms recorded during a shot with an 80-kV composite charge voltage on the module. As indicated above the graph, the crowbar switch was triggered  $1.8 \mu\text{s}$  after the Shiva Star module was discharged, slightly before the load current reached its peak (which was observed to occur at  $\sim 2.85 \mu\text{s} \pm 0.05 \mu\text{s}$ ). For this test shot a peak current of  $\sim 1.2 \text{ MA}$  was achieved. More mention will be made of the oscillations observed in the load current waveforms in the following subsection.

The goal for the peak current in the FRX-L theta coils has been approximately 1.5 MA, which would allow the desired magnetic field to be generated within their bore for compressing the plasma and forming the field reversed configuration. Fig. 10 shows a graph of the peak currents from three shots, all having the same crowbar trigger delay of  $1.8 \mu\text{s}$ , plotted as a function of the module composite charge voltage. This graph indicates that a slightly higher charge voltage ( $\sim 99 \text{ kV}$ ) will be required to achieve the desired 1.5 MA, if the trigger delay of  $1.8 \mu\text{s}$  is maintained. (However, because the theta coils on the FRX-L experiment have an inductance slightly less than that of the test load, the actual charge voltage may not be quite as high.)

### B. Flashover in Cable Headers

The cable headers were monitored very closely for signs of flashover as the charge voltage on the Shiva Star module was increased. As was noted at the beginning of Section II, the original cable header on the Colt bank was observed to flash over quite regularly at voltages above  $60\sim 70 \text{ kV}$ , even when  $\text{SF}_6$  was flowed into the bottom of the cable header. With the crowbar switch in place and in operation, the voltage hold-off requirements for the crowbar cable header are somewhat lessened, as the only time there is significant voltage across the header is right after the module is triggered (the cable header is shorted out after the crowbar switch is triggered). However if flashover were to occur, it is significantly more troublesome and time consuming to clean because of the crowbar switch on top.

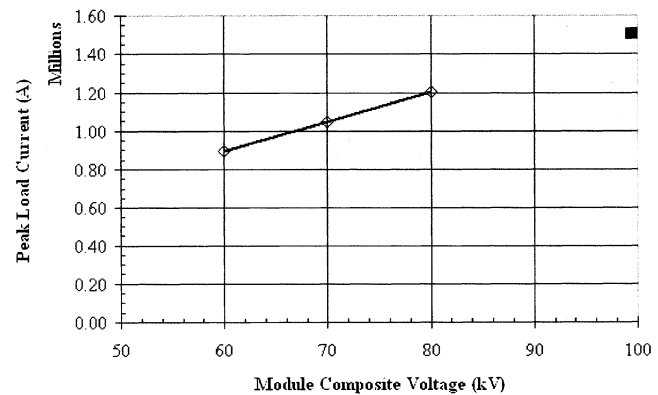


Fig. 10. Peak load currents from several test shots plotted as a function of the composite charge voltage on the capacitor module. The solid square in the upper right corner indicates the charge voltage (99 kV) needed to achieve a peak current in the load of 1.5 MA.

During the test shots at AFRL, flashover was observed to occur only two times, both on 80 kV test shots, and during these two shots it was observed in the load cable header only. Inspection of the header following the second shot showed several areas of discoloration on the Mylar surface. At this point the load and load cable header were disassembled completely, and the insulating Mylar sheets were cleaned. When reassembling, the corners of the load inductor mounting tabs (that attached to the cable header) and their copper gaskets were rounded off, Noalox, which had previously been used on the copper gaskets to improve electrical contact with the aluminum header bus bar and the stainless steel inductor tab, was not used this time, and the header was sealed more thoroughly to allow for better filling with  $\text{SF}_6$ . (Noalox was felt to have perhaps been creating additional flashover problems, because traces of it were found out on the Mylar when the header was disassembled. Either due to mechanical shock or localized breakdown around the metal joints, the drops of Noalox could have been ejected out onto the Mylar, and because of its conductive properties, the Noalox could enhance the likelihood of a surface discharge occurring directly across the Mylar surface.) After these changes were made, no further evidence of flashover was observed in any of the subsequent shots, which were all performed with an 80 kV charge voltage.

### C. Charge Flow Through the Crowbar Switch

An item of concern as the crowbar switch was being designed was the amount of charge that the rail-gap switches must conduct for each shot. The quad set of rail-gap switches is rated at 40 C, but as the charging voltage of the Shiva module approaches moderate to high values, depending on the test load inductance, the charge flow was expected to exceed this limit. Personnel at Maxwell Technologies familiar with rail gap performance noted that studies on how the rail-gap switches will handle excessive charge flow have not really been conducted up to this point, and therefore information concerning the issue is sketchy [4]. It was stated, however, that as long as the switches are able to operate with good multichannel arcing across the gaps and not with just a single-channel arc, there should be no significant damage that would occur to the switches.

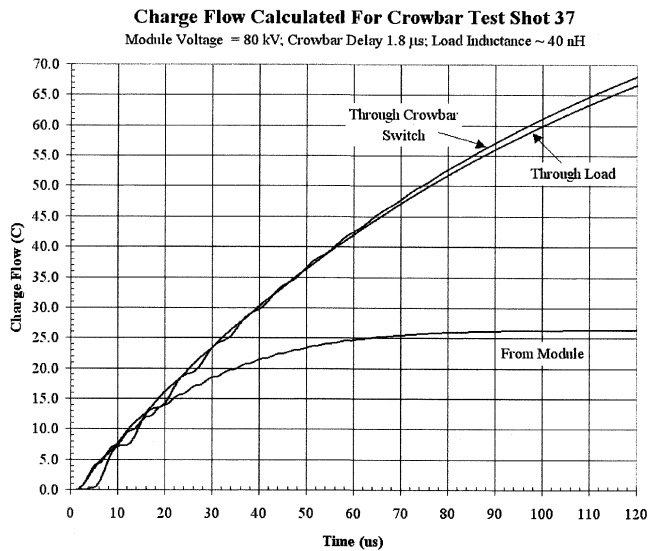


Fig. 11. Charge flow from the capacitor module, through the crowbar switch, and through the load as a function of time during Test Shot 37. These waveforms were obtained by integrating the current waveforms shown in Fig. 9. The waveform records captured by the oscilloscopes ended at approximately 120  $\mu$ s, but it appears that charge flow through the load and crowbar switch exceeded 70 Coulombs by the end of the shot.

A plot of the charge flow through various components of the test circuit during Test Shot 37 (obtained by integrating each of the current waveforms in Fig. 9) is shown in Fig. 11. Of particular interest, of course, is the charge flow through the crowbar switch. As can be seen from the plot, the total charge flow through the crowbar switch appears to exceed 70 Coulombs. Despite the excessive charge flows during these shots, no excessive wear on the switch rails (beyond that which occurs during normal use) or damage to the housings was observed, thus supporting the expectations of Maxwell personnel mentioned above. The photo in Fig. 12 shows one of the rail gap switches just prior to cleaning after Test Shot 30. At this point the crowbar switch had been fired 16 times, and charge flow exceeded the rated flow in three of the shots. In the following 10 shots, the rated charge flow was exceeded each time, with charge flows ranging from  $\sim 47$  Coulombs to over 70 Coulombs, yet condition of the rail-gap switches appeared very much like that shown in Fig. 12 at the time of their next cleaning. The conclusion that can be drawn is that a significantly higher charge can be run through the crowbar switch than what has been rated by the rail gap manufacturer with the recommendation that the rail gaps must be cleaned more frequently—perhaps after every 10 to 20 such shots—to ensure that pre-fire of the crowbar switch does not occur. The frequency of cleaning can be decreased somewhat if the theta coil discharge in the FRX-L experiment turns out to be more resistive, thereby bringing the current to zero faster after the Colt bank is triggered and reducing the total charge flow through the rail gaps in each shot.

#### D. Load Current Oscillations and Crowbar Switch Inductance

Returning to Fig. 9, the graph in this figure shows that in Test Shot 37 oscillations were present in the load current waveform

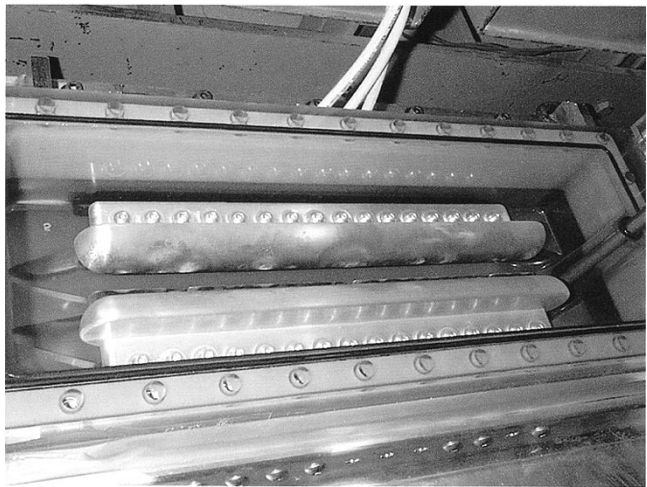


Fig. 12. Photo of one of the crowbar rail-gap switches prior to the first cleaning after Test Shot 30. Despite the high charge flows in each shot, no evidence of damage or excessive wear was observed. The light coating found on the bottom and sides of the switch housing (not easily seen in the black-and-white photo) builds up with each shot, though, and makes it necessary to clean the switches frequently to prevent the possibility of pre-fire of the crowbar switch.

after crowbarring. The amplitude of the oscillations tended to be even greater in earlier test shots where the smaller load inductance (10 nH) was used. These oscillations are caused by the inductance of the crowbar switch and its associated buss work as that inductance is switched into the circuit when the crowbar fires. A figure of merit that has been used to describe the amplitude of the current oscillations is the ratio of the current at the first minimum after the peak to the current at the peak:  $I_{\min,1}/I_{\text{peak}} = R_i$ . In the case of Test Shot 37,  $R_i = 0.579$ .

Using Spectrum Software's circuit simulation program, *Micro-Cap*, the crowbar test setup circuit was modeled, and estimates were obtained for the crowbar inductance by matching the calculated load current waveforms with the waveforms obtained from the test shots. For Test Shot 29, where the composite charge voltage of the Shiva module was only 60 kV, an inductance of  $\sim 12.1$  nH was inferred for the crowbar circuit, and for Test Shot 37, where the charge voltage was 80 kV, an inductance of  $\sim 10.1$  nH was estimated.

As the delay in triggering the crowbar switch was increased, thereby moving the trigger point closer to the time of the current peak, the amplitude of the oscillations in the load current waveform increased rather significantly. Fig. 13 shows the current waveforms from Test Shot 38 as an example. For this shot the trigger delay was increased to 2.2  $\mu$ s, and the ratio  $R_i$  dropped to 0.486.

The graph in Fig. 14 highlights the peak current, the current at the first minimum, and the ratio of the two from several shots as a function of the crowbar trigger delay time. This graph illustrates that the trend of oscillation growth continues as the trigger time is moved closer to the time of the current peak. A probable explanation for this trend is that as the crowbar switch is triggered closer to the time of the current peak, multi-channeling in the rail gaps becomes poorer due to there being a lower voltage across the rails at this time. The inductance of the crowbar switch thus becomes larger, and as a result the oscillation amplitude grows.

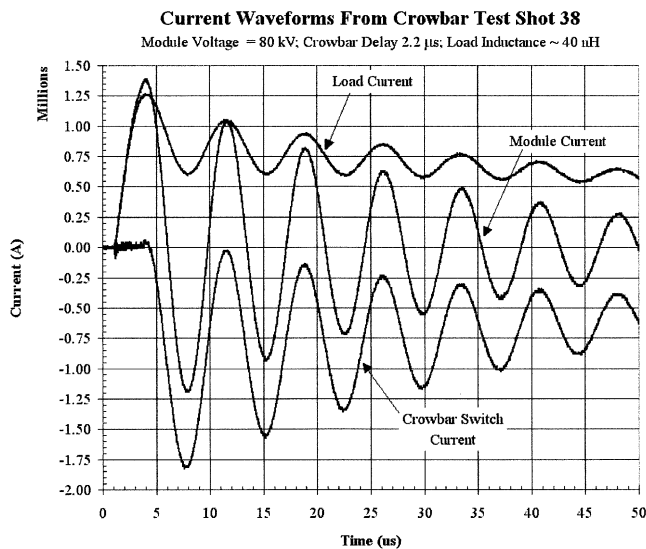


Fig. 13. Current waveforms obtained from Test Shot 38. By increasing the trigger delay by  $0.4 \mu\text{s}$ , the amplitude of the load current oscillations increased by  $\sim 17\%$  and the ratio  $R_i$  decreased from 0.579 to 0.486.

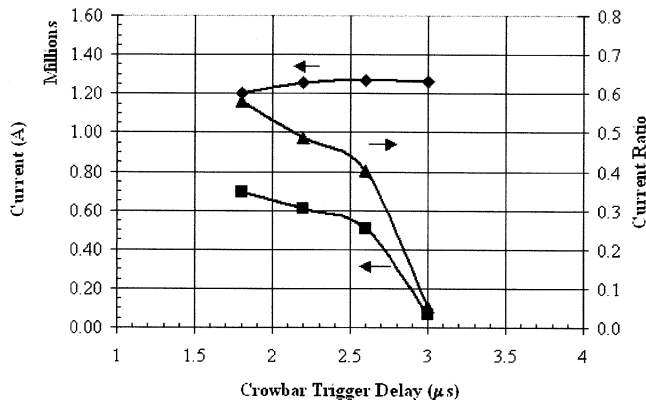


Fig. 14. Data for peak load current, load current at the first minimum, and the ratio of  $I_{\min,1}/I_{\text{peak}}$  ( $=R_i$ ) taken from several shots with varying crowbar trigger delay times. The load inductance for these test shots was  $40 \text{ nH}$ , and the composite charge voltage was  $80 \text{ kV}$ . The amplitude of the oscillations increased as the crowbar trigger time approached the time of the current peak, while the value of the peak current remained relatively unchanged.

Since the peak load current does not increase greatly as the crowbar trigger time is moved closer to the time of current peak, whereas the oscillations continue to grow, there is no advantage to setting the crowbar trigger delay for longer than  $1.8 \mu\text{s}$ . Delay times shorter than  $1.8 \mu\text{s}$  were not investigated for this load inductance or module charge voltage, however based on earlier test shots the peak load current is likely to begin dropping more rapidly as the crowbar trigger delay is reduced below  $1.8 \mu\text{s}$ . Thus,  $1.8 \mu\text{s}$  appears to be the optimum delay time for triggering the crowbar switch. A possible method for reducing the hardware-related inductance and therefore the amplitude of the oscillations in the load current waveform is discussed in the next section.

#### IV. POSSIBLE MODIFICATIONS TO LOWER SWITCH INDUCTANCE

Other design arrangements for the crowbar switch exist that would allow for lower crowbar inductance, designs in which the

crowbar rail gaps are mounted between two parallel bus plates in the same way that the main discharge gaps are mounted on the front of the Shiva Star modules. In these schemes, the rail gaps are located two on each side of the module or on an extension to the bus plates that would place the four rail gaps beside the main discharge gaps. The present design was chosen, however, because it required very little additional hardware to the cable header, and no changes to the existing Shiva module hardware (bus plates) were needed. Analysis and experiments *may* show that the field-reversed configuration is stable enough such that the oscillations in the crowbarred reverse discharge current (reverse magnetic field) will not significantly affect its formation and lifetime. However, if the current oscillations are found to have an adverse affect on the FRC, examination of the present crowbar switch design shows that there are some relatively minor changes can be made to reduce the crowbar switch inductance and thereby reduce the amplitude of the current oscillations.

A cross-sectional diagram of the crowbar switch configuration with the proposed changes indicated is presented in Fig. 15. At present the crowbar rail gaps are approximately  $9/16 \text{ in.}$  above the bottom edge of the support brackets holding them; if the rail gaps are moved down until their bottom edge is even with the support brackets, and if both the lower face of the support brackets and the rail gaps are moved down by an additional  $0.5 \text{ in.}$ , as shown in the figure, then calculations show that the inductance of the crowbar switch can be reduced by approximately  $4.47 \text{ nH}$ .

To determine what kind of effect reducing the switch inductance by this amount would have on the load current waveform, some simulations of the crowbar test circuit were performed again using *Micro-Cap*. Fig. 16 shows the first  $18\sim 19 \mu\text{s}$  of the load current waveform from Test Shot 37 along with the calculated load current waveform provided by *Micro-Cap*. Assuming a switch inductance of  $10.1 \text{ nH}$ , fairly good agreement is obtained between the *Micro-Cap* calculation and the experimental result, at least until  $t = 13\sim 14 \mu\text{s}$ . When the total crowbar switch inductance is reduced by  $4.47 \text{ nH}$ , the third trace in Fig. 16 is obtained. This trace has a slightly lower peak current,  $\sim 1.18 \text{ MA}$ , however the value of the current at the first minimum has risen to  $\sim 800 \text{ kA}$ , resulting in a ratio  $R_i$  of 0.68. (Recall that  $R_i$  for Test Shot 37 is 0.579.) As indicated in Fig. 15, the only hardware components that would need to be modified in order to obtain this improvement are the angle brackets supporting the crowbar rail gaps above the cable header. Thus, this improvement could be made at relatively little cost and down time.

#### V. SUMMARY AND EVALUATION OF PERFORMANCE

The crowbar tests were performed with charge voltages of up to  $80 \text{ kV}$  on the Shiva capacitor bank module, during which currents of up to  $\sim 1.25 \text{ MA}$  were crowbarred. No evidence of flashover in the crowbar or load cable headers was observed when the headers were adequately filled with  $\text{SF}_6$ . In order to achieve the desired load current (theta coil current) of  $1.5 \text{ MA}$ , however, the charge voltage will have to be increased to slightly higher values of  $\sim 100 \text{ kV}$ . As long as an adequate filling of

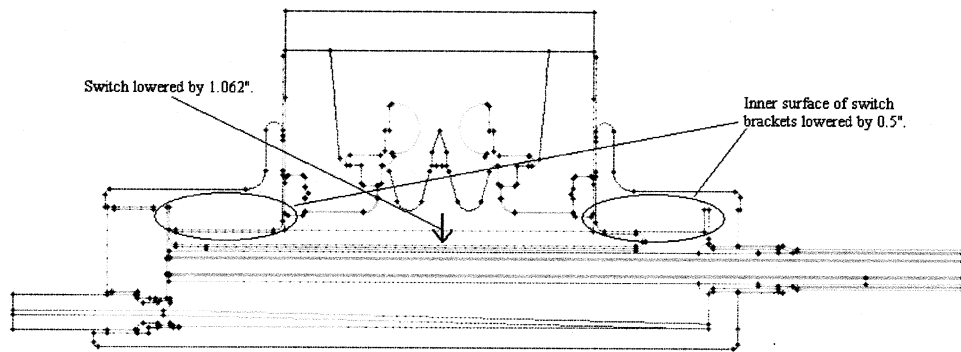


Fig. 15. Cross-sectional diagram of the crowbar switch and crowbar cable header. Indicated in the diagram are changes that could be made to the supporting angle brackets on the rail gaps to reduce the switch inductance by  $\sim 4.47$  nH.

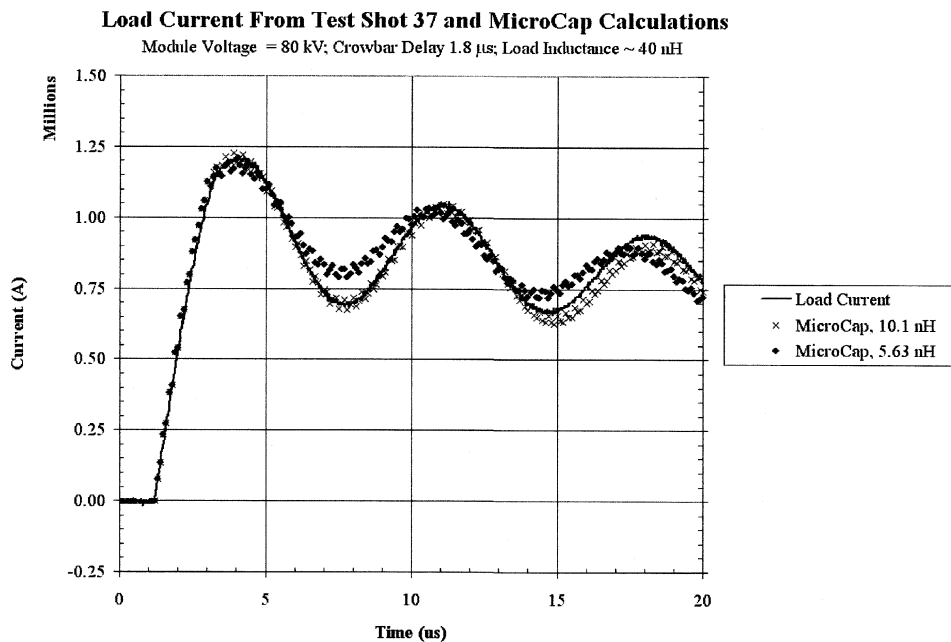


Fig. 16. The load current waveform from Test Shot 37 plotted with the load currents calculated by *Micro-Cap* in simulations of the crowbar test circuit before and after the crowbar switch inductance is reduced by 4.47 nH. For the lower crowbar switch inductance, the first minimum in the load current waveform has risen to  $\sim 800$  kA, and though the peak current has dropped slightly, the ratio  $R_i$  has become 0.68.

$SF_6$  can be sustained within the cable headers, however, voltage hold-off should still be able to be maintained, particularly in the crowbar cable header where the high initial voltage is present only very briefly as the capacitor module is first discharged. Redesigning the support brackets for the crowbar rail gaps such that the rail gaps are positioned somewhat closer to the cables in the crowbar cable header can likely reduce inductance in the crowbar switch and its related buss work and also reduce the amplitude of the oscillations in the load current.

After the completion of the tests at AFRL, the crowbar switch and all relevant hardware were moved to the FRX-L facility at LANL and prepared for operation. FRC formation experiments are now scheduled to begin there very soon. Following successful completion of these experiments at LANL, plans have been made to assemble an identical experimental setup back at AFRL. Here the FRC would be formed, translated axially into the bore of a solid liner, and then the Shiva Star capacitor bank would be used to implode this liner.

#### ACKNOWLEDGMENT

The authors wish to thank D. Henley for his assistance with machining and fabricating various components for the test setup at AFRL, M. Keys for her work in preparing the technical drawings of the crowbar switch assembly and related hardware, B. Martinez for his assistance with assembling the crowbar switch hardware at AFRL for the initial tests and with reassembling it again at LANL, and R. Sedillo for his help with performing the various test shots at AFRL.

#### REFERENCES

- [1] D. J. Rej, "Dynamic processes in field-reversed-configuration compact toroids," in *Proc. Course and Workshop Held at Villa Monastero: Physics of Mirrors, Reversed Field Pinches and Compact Tori*, S. Ortolani and E. Sindoni, Eds. Varenna, Italy, Sept. 1–11, 1987, vol. II, pp. 499–518.
- [2] K. F. Schoenberg *et al.*, "Magnetized target fusion: A proof-of-principle research proposal," Los Alamos Nat. Lab. Proposal, LA-UR-98-2413, 1998.

- [3] T. Naff, private communication.  
 [4] R. Miller, private communication.



**Chris Grabowski** was born in Dayton, OH, on October 8, 1966. He received the B.S. degree in electrical engineering from Texas Tech University, Lubbock, in 1988 and the M.S. and Ph.D. degrees in electrical engineering from the University of New Mexico, Albuquerque, in 1990 and 1997, respectively.

During 1991 and part of 1992, he worked as a Research Student in the Pulsed Power Laboratory at Kumamoto University, Kumamoto, Japan, studying inductive energy storage pulsed power generators.

After graduation, he worked as a Postdoctoral Researcher at both the Weizmann Institute of Science in Rehovot, Israel, and at Cornell University, Ithaca, NY, studying plasma spectroscopy and high-power traveling wave tube amplifiers, respectively. Currently, he is a senior staff engineer with Science Applications International Corporation, Albuquerque, where he has had the opportunity to work on a wide variety of pulsed power projects.



**James H. Degnan** (A'90–M'99–SM'99) received the Ph.D. degree in physics in 1973 from the Department of Physics and Astronomy, University of Pittsburgh, PA, where he did his thesis work on experimental nuclear reaction studies.

Since 1973, he has been with the Air Force Research Laboratory (AFRL) and its predecessors, Air Force Weapons Laboratory and Phillips Laboratory. There he designed, conducted, and directed research on high energy density plasmas, radiation diagnostics, and pulsed power. His recent work includes mag-

netic pressure implosions of cylindrical and spherical metal shells for plasma compression. He is presently a senior physicist (GS-15 = DR-IV) and Technical Advisor of the Pulsed Power Branch (DEHP) in the High Power Microwave Division of the Directed Energy Directorate of the Air Force Research Laboratory (AFRL/DEH).

**T. Cavazos** (M'85), photograph and biography not available at the time of publication.



**Donald G. Gale** received the B.S. degree in mechanical engineering from Cal Poly, San Luis Obispo, in 1976.

He is a Registered Professional Mechanical Engineer, in the state of California since 1977. He is a Certified arc welder in the Los Angeles County Department of Building and Safety, since 1971. He has 14 years of experience in structural design/stress analysis in the commercial nuclear power industry, and 13 years of experience in component design for pulsed power and high-power microwave applications. He is

skilled in machining, welding, and fabrication techniques. Currently, he is specializing in explosive flux compression generators.

**C. Gilman** (M'86), photograph and biography not available at the time of publication.

**W. Sommars**, photograph and biography not available at the time of publication.

**Tom P. Intrator** grew up in and around New York City. He received the B.S. degree in physics from the State University of New York, Albany, in 1976, and the M.S. and Ph.D. degrees in physics from the University of Colorado, Boulder, in 1981 and 1982, respectively.

Recently, he joined Los Alamos National Laboratory (LANL), Los Alamos, NM, as a Member of Technical Staff and is leading the effort to create a high-density field reversed configuration for magnetized target fusion. He also has built a magnetic reconnection scaling experiment at LANL to study astrophysics issues in the laboratory. After research at the Cyclotron at the University of Colorado - Boulder, the tantalizing dream of a fusion power solution to our energy crisis inspired a plasma physics career. Subsequent physics, engineering, and teaching work at the University of Wisconsin included a host of basic physics tabletop experiments and nonlinear wave particle interactions in magnetic fusion devices such as mirrors, tokamaks, and a reversed field pinch. A sojourn as visiting scientist at Bell Laboratories, Murray Hill, NJ, in 1987 was followed by a year as Visiting Professor at the Université de Grenoble, France, in 1989.

**J. Martin Taccetti** (M'88) was born in Buenos Aires, Argentina. He received the B.S. degree in physics from SUNY, Stony Brook, in 1990, and the Ph.D. degree from the University of Maryland, College Park, in 1998.

He performed his thesis work on free-electron lasers at the Naval Research Laboratory, Washington, DC. He is presently a staff member of the Plasma Physics group, Los Alamos National Laboratory, Los Alamos, NM, where his research involves the study of magnetized target fusion as an approach to fusion.

**B. Waganaar**, photograph and biography not available at the time of publication.

**R. E. Siemon**, photograph and biography not available at the time of publication.



**Glen A. Wurden** (M'94–SM'00) received the Ph.D. degree in astrophysical sciences (plasma physics) from Princeton University, Princeton, NJ, in 1982.

He is the team leader for magnetic fusion experiments in the P-24 Plasma Physics Group at Los Alamos National Laboratory, Los Alamos, NM. His interests include making fusion energy a reality in our lifetime, and he is an expert in plasma diagnostics, collaborative experiments, and a variety of magnetic confinement concepts

Dr. Wurden is a member of the American Physical Society and Phi Beta Kappa.